frontiers in Chemistry

ORIGINAL RESEARCH
published: 15 October 2020
doi: 10.3389/fchem.2020.00803

Detection of Pb(II): Au Nanoparticle Incorporated CuBTC MOFs

Gajanan A. Bodkhe[1†], Bhavna S. Hedau[1†], Megha A. Deshmukh[1], Harshada K. Patil[1], Sumedh M. Shirsat[2], Devdatta M. Phase[3], Krishan K. Pandey[4] and Mahendra D. Shirsat[1]*

[1] RUSA Center for Advanced Sensor Technology, Department of Physics, Dr. Babasaheb Ambedkar Marathwada University, Aurangabad, India, [2] Department of Electronics and Telecommunication Engineering, Jawaharlal Nehru Engineering College, Aurangabad, India, [3] UGC-DAE Consortium for Scientific Research, University Campus, Indore, India, [4] High Pressure and Synchrotron Radiation Physics Division, Bhabha Atomic Research Center, Mumbai, India

In the present investigation, copper benzene tricarboxylate metal organic frameworks (CuBTC MOF) and Au nanoparticle incorporated CuBTC MOF (Au@CuBTC) were synthesized by the conventional solvothermal method in a round bottom flask at 105°C and kept in an oil bath. The synthesized CuBTC MOF and Au@CuBTC MOFs were characterized by structure using X-ray diffraction (XRD) spectroscopic methods including Fourier Transform Infrared spectroscopy, Raman Spectroscopy, X-ray Photoelectron Spectroscopy (XPS), and Energy dispersive spectroscopy (EDS). We also characterized them using morphological techniques such as Field emission scanning electron microscopy (FE-SEM), and electrochemical approaches that included cyclic voltammetry (CV) and electrochemical impedance spectroscopy (EIS). We examined thermal stability by thermogravimetric analysis (TG/DTA) and N_2 adsorption—desorption isotherm by Brunauer-Emmett-Teller (BET) surface area method. Both materials were tested for the detection of lead (II) ions in aqueous media. Au nanoparticle incorporated CuBTC MOF showed great affinity and selectivity toward Pb^{2+} ions and achieved a lower detection limit (LOD) of 1 nM/L by differential pulse voltammetry (DPV) technique, which is far below than MCL for Pb^{2+} ions (0.03 μM/L) suggested by the United States (U.S.) Environmental Protection Agency (EPA) drinking water regulations.

Keywords: differential pulse voltammetry (DPV), electrochemical sensor, gold nanoparticles, metal organic frameworks, CuBTC MOF

OPEN ACCESS

Edited by:
Daojun Zhang,
Anyang Normal University, China

Reviewed by:
Fugang Xu,
Jiangxi Normal University, China
Xuan Zhang,
Donghua University, China

***Correspondence:**
Mahendra D. Shirsat
mdshirsat.phy@bamu.ac.in

[†] These authors have contributed equally to this work

Specialty section:
This article was submitted to Supramolecular Chemistry, a section of the journal Frontiers in Chemistry

Received: *27 May 2020*
Accepted: *30 July 2020*
Published: *15 October 2020*

Citation:
Bodkhe GA, Hedau BS, Deshmukh MA, Patil HK, Shirsat SM, Phase DM, Pandey KK and Shirsat MD (2020) Detection of Pb(II): Au Nanoparticle Incorporated CuBTC MOFs. Front. Chem. 8:803. doi: 10.3389/fchem.2020.00803

INTRODUCTION

Heavy metal ions are a major water pollutant caused by sewage from chemical industries and various other sources (Singh et al., 2011; Maleki et al., 2019). Some of the more toxic heavy metal ions include Pb(II), Cu(II), Hg(II), Co(II), etc. (Meena et al., 2005). The accumulation of heavy metallic ions results in severe health issues, damage to the ecosystem (Wu et al., 2010), and significant damage to the environment (Fu and Wang, 2011). It is well-known that Pb(II) is toxic for human and aquatic health (Deshmukh et al., 2018b), causing health issues which include memory damage, muscle fatigue, neurotic diseases, damage to the liver and kidneys, reduction in hemoglobin formation, infertility, and abnormalities in pregnancy, amongst other concerning side effects (Meena et al., 2005). There is an urgent need to detect and remove these pollutants from water, by introducing highly sensitive and selective sensing materials. Various technologies have been introduced for highly sensitive heavy metal ion detection, namely liquid chromatography (Ali and Aboul-Enein, 2002), solid-phase extraction coupled with atomic absorption spectroscopy

(Faraji et al., 2010), and atomic emission spectroscopy. However, these methods are very expensive, time-consuming, and require experts to operate the instruments (Quang and Kim, 2010).

Researchers are also dedicating efforts to developing heavy metal ions sensors in other modalities, such as the fluorescent (Neupane et al., 2011), Field Effect Transistors (FETs) (Cobben et al., 1992), Surface-Enhanced Raman Scattering (SERS) (Tan et al., 2012), Surface Plasmon Resonance (SPR) (Forzani et al., 2005), colorimetric (Hung et al., 2010), and electrochemical sensors (Deshmukh et al., 2018c,d). Most of these techniques are challenging due to the high cost of the laboratory facilities that they require. Modalities such as electrochemical sensors are, on the other hand, an ideal and prominent option due to advantages such as the fact that they require simple and cost-effective instruments and have faster analytical responses (Kimmel et al., 2011). Researchers have explored various materials for the detection of heavy metal ions in aqueous media in electrochemical modality, for example considering organic conducting polymers (OCPs) (Deshmukh et al., 2018e), carbon nanotubes (CNTs) (Deshmukh et al., 2018e; Maleki, 2018), metal oxides (Hwang et al., 2008), graphene (Dai et al., 2016), bioreceptors (Cui et al., 2015), metal nanoparticles (Kim et al., 2001), and metal organic frameworks (MOFs) (Roushani et al., 2016), among others.

Recently, researchers have had an interest in an efficient material called Metal Organic Frameworks (MOFs) due to versatile physical and chemical properties, high porosity, ultrahigh surface area, high electrical transfer rate, high crystallinity, evenly element doping, and abundant metal sites (Bodkhe et al., 2019), among other benefits. MOFs are generally composed of a central metal ion and organic linker resulting in crystalline and porous materials. These properties make them useful in versatile applications as a catalyst (Lee et al., 2009), potential biomedical applications (Wuttke et al., 2017), sensors (Rauf et al., 2020), gas storage (Chen et al., 2020), and separation (Lin et al., 2020).

However, the sensing properties of MOFs can be enhanced by combining them with other efficient materials (Liu et al., 2018). Nanocomposites (Maleki et al., 2016) are a combination of various materials that overcome or improve deficiencies in the parent material (Maleki et al., 2018), which makes them advantageous when used in sensors. The episodic structure of MOFs makes them an attractive candidate for the encapsulation of metal nanoparticles (such as Ag, Pt, Cu, and Au, etc.) due to increased control of the regular distribution of nanoparticles and enhancement of the stability of NPs (Butova et al., 2018). The porous structure of MOFs make NPs accessible to the environment, meaning they are good candidates for use in sensors. Among all nanoparticles, gold (Au) nanoparticles have shown better results when incorporated in MOFs, showing carbon monoxide oxidation (Jiang et al., 2009), alcohols oxidation (Ishida et al., 2008), hydrazine electrocatalytic oxidation (Han et al., 2015), and a reduction of 4-hydroxynitrobenzene (Ke et al., 2015).

Inspired by these reports, this study exploited various properties of copper benzene tricarboxylate (CuBTC) MOF to synthesize the Au nanoparticles incorporated CuBTC (henceforth referred to as Au@CuBTC). CuBTC MOF contains Cu(II) central metal ion and benzene tricarboxylic acid as an organic linker. CuBTC MOF is the most explored MOF. The CuBTC MOF shows good electrochemical performance and electro catalytic activity which makes them suitable for electrochemical sensors using hydrazine (Meng et al., 2019), nitrite (Saraf et al., 2016), hydroquinone, catechol (Zhou et al., 2015), ammonia (Travlou et al., 2015), and H_2O_2 (Zhang et al., 2013; Golsheikh et al., 2020). This study observed that pure CuBTC MOF does not show any electrochrochemical response to Pb(II) ions at 0.01 mM/L concentration. However, Au@CuBTC MOF shows an electrochemical response up to 1 nM/L concentration, which is far below the MCL level of Pb(II) ions. The porous structure of CuBTC provided maximum surface area and Au NPs enhanced electrocatalytic activity, which makes the material a highly sensitive and selective electrochemical sensor for Pb(II) ions.

EXPERIMENTAL

Materials and Chemicals

All the reagents and chemicals were analytical grade and used without purification. Benzene-1,3,5-tricarboxylic acid (BTC), Copper nitrate trihydrate ($Cu(NO_3)_2$,$3H_2O$), and N, N dimethyl formamide (DMF) purchased from Sigma Aldrich. Chloroauric acid, Hydrazine hydrate, hydrochloric acid, sodium acetate, acetic acid, sodium hydroxide, hydrochloric acid, and ethanol purchased from Molychem, India.

Synthesis of CuBTC MOF

The CuBTC MOF was synthesized as per the reported method (Marx et al., 2011). 2.252 gm of Copper nitrate trihydrate [$Cu(NO_3)_2$, $3H_2O$] was mixed with 50 ml of deionized water and benzene-1,3,5-tricarboxylic acid (BTC) (0.982 gm) in 50 ml of DMF, prepared separately and mixed with constant stirring at room temperature. The precursor solution was transferred into a 250 ml round-bottom flask and kept in an oil bath at 105°C for 4 h. After completion of the reaction, CuBTC MOF crystals were observed at the bottom of the round-bottom flask. After cooling at room temperature, CuBTC MOF crystals were washed with deionized water and ethanol three times each to remove unreacted reactants. The filtered CuBTC MOF was kept for activation at 120°C for 12 h to remove coordinated solvent molecules from the pores (Bodkhe et al., 2019). After activation, the color of CuBTC changed from faint blue to dark blue. The activated CuBTC MOF was stored in air tight sample containers for further use.

Synthesis of Au@CuBTC MOF

Gold (Au) nanoparticle precursor solution was prepared separately, as reported in other studies (Yadav et al., 2018). Chloroauric acid ($HAuCl_4$) (0.71 mM) was used as the gold (Au) source, mixed with 0.1 M hydrochloric acid (HCl) in D. I. water, with 0.71 mM hydrazine hydrate then added slowly. This solution was stirred for 30 min and sonicated for 5 min. The synthesis procedure for Au@CuBTC MOF is the same as CuBTC MOFs. In the precursor solution of CuBTC, the Au NPs precursor solution

was added slowly then stirred for 30 min and sonicated for 5 min. This solution was transferred into a 250 ml round bottom flask and kept in an oil bath for 4 h at 105°C. Au@CuBTC MOF was cooled at room temperature and washed with deionized water and ethanol three times each. The filtered Au@CuBTC MOF activated at 120°C for 12 h and stored for further use.

Preparation of CuBTC and Au@CuBTC MOF Electrode

Glassy carbon electrode (GCE) was used as an electrode for all electrochemical experiments. The GCEs were carefully polished with alumina powder slurries of 1, 0.3, and 0.05 μ, respectively, to get a mirror like surface. Then the GCE was ultrasonicated and washed with acetone and D.I. water sequentially. The preconditioning of bare GCE was performed in 0.5 M of H_2SO_4 solution using the cyclic voltammetry (CV) technique in the potential window of −0.35 to 1.5 V at a scan rate of 100 mV/s until stable voltammogram was observed.

The pure CuBTC and Au@CuBTC MOF were properly mixed in diluted nafion in acetone. The prepared suspension of pure CuBTC and Au@CuBTC MOF were drop cast on GCE electrodes and dried at room temperature, then used for electrochemical experiments.

Electrochemical Detection of Lead (Pb^{2+}) Ions

The Pb^{2+} ions solution was prepared in acetate buffer at pH 5.0 using $Pb(NO_3)_2$ (Pb^{2+} ions source), $Pb(NO_3)_2$ mixed properly, with constant stirring for 30 min. The Pb^{2+} ions solution was prepared at a higher concentration and used as a stock solution, a lower concentration was prepared by diluting it with the addition of a buffer solution. Electrochemical detection of Pb^{2+} ions was carried out on CHI 660C electrochemical workstation by the differential pulse voltammetry technique. The GCE modified electrodes of pure CuBTC and Au@CuBTC were used as the working electrode, platinum served as the counter electrode, while Ag/AgCl were used as a reference. Initially, the accumulation of Pb^{2+} ions on GCE modified electrodes was carried out by dipping the modified electrode for 5 min at constant pH of 5.0, then DPV in another buffer (pH = 5.0) was carried out in the potential from 0 to (−1) volts.

Apparatus and Instruments

Powder X-ray diffraction (XRD) measurements were performed on a Bruker D8 Advance Diffractometer with Cu kα1 radiation (λ = 1.5406). The Fourier Transform Infrared (FTIR) spectrum was recorded on Bruker Alpha FTIR in ATR mode with the ZnSe window in the range of 500 to 4,000 cm^{-1}. Nitrogen adsorption-desorption isotherm measurements were carried out on Autosorb iQ Station 1 instrument at 77 K and all samples were degassed at 150°C in a helium environment. The X-Ray Photoelectron studies were carried out on the XPS facility available at Raja Ramanna Center for Advanced Technology (RRCAT), Indore, India.

Thermogravimetric measurements were carried out on Shimadzu to take the DTG-60H model from room temperature to 1,000°C, with a scan rate of 10°C/min in the nitrogen environment. The Raman spectrum of all the samples was recorded on a Renishaw inVia reflex Raman microscope in the spectral range of 90 to 2,000 cm^{-1} at 532 nm laser excitation wavelength. Cyclic Voltammetry (CV) and Electrochemical Impedance Spectroscopy (EIS) measurements were carried out on a CHI 660C electrochemical workstation with platinum (Pt) foil, Ag/AgCl as counter and reference electrodes, respectively. The CV was recorded in the potential range of −0.8–0.5 V in 10 mM $[Fe(CN)6]^{3-/4-}$ solution containing 0.1 M KCl solution at a scan rate of 100 mV/S. EIS measurements were taken in the frequency range of 0.01–0.1 MHz in the 0.1 M KCl solution. Electrochemical sensing experiments were performed in acetate buffer at 5.0 pH by differential pulse voltammetry (DPV) technique on CHI 660C electrochemical workstation having Ag/AgCl and Pt foil as reference and counter electrodes respectively.

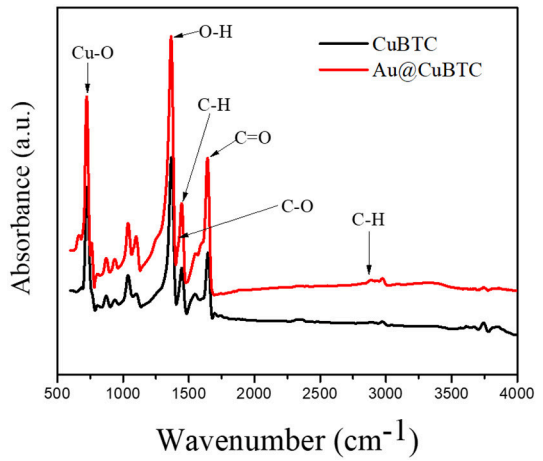

FIGURE 1 | FTIR Spectra of as-synthesized CuBTC MOF and Au@CuBTC MOF.

RESULTS AND DISCUSSION

Materials Characterization

Fourier Transform Infrared Spectroscopy Analysis

As-synthesized CuBTC MOF and Au@CuBTC MOF were characterized by FTIR spectroscopy as shown in **Figure 1**. In CuBTC MOF, the presence of asymmetric C-H stretching vibration and asymmetric stretching of the carboxylic groups confirmed by bands present at 2,890 cm^{-1} and 1,446 cm^{-1} (Dastan et al., 2016). The absorption band at 730 cm^{-1} attributed to Cu-O stretching vibration. The absorption peaks at 1,640 cm^{-1} attributed to the stretching of $V_{C=O}$ while the band at 1,446 cm^{-1} were attributed to the stretching of V_{C-O}. The band at 1,373 cm^{-1} indicated that there was a bending of O-H functional groups (Lin et al., 2014) and confirms the CuBTC MOF. The FTIR spectra of Au nanoparticle incorporated CuBTC does not show any difference in peak position in FTIR spectra, but there was an increase in absorption of the IR spectrum in Au nanoparticle incorporated CuBTC MOF. This confirms

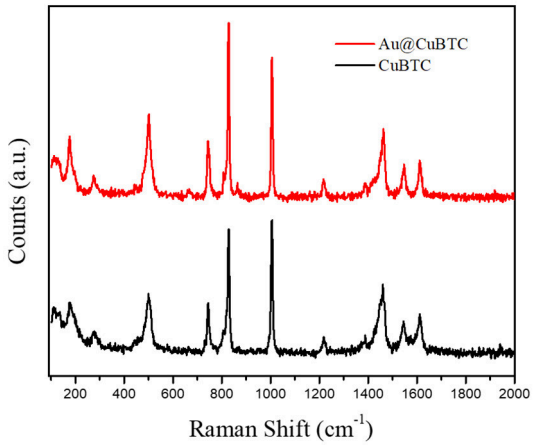

FIGURE 2 | The Raman Spectra of as-synthesized CuBTC MOF and Au@CuBTC MOF.

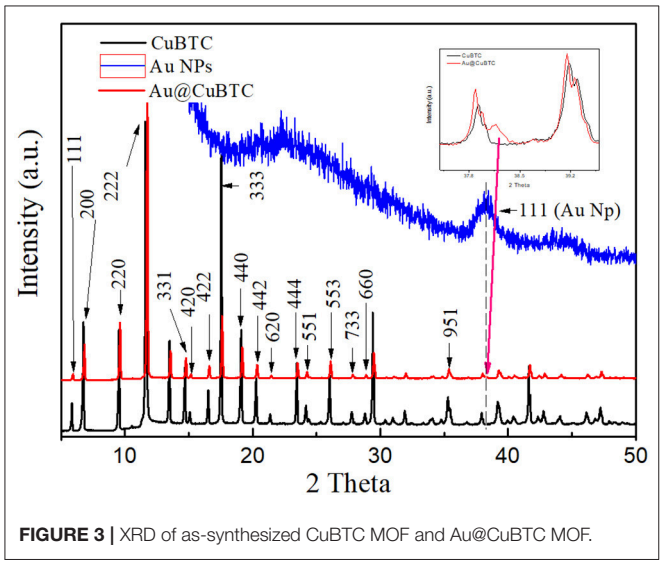

FIGURE 3 | XRD of as-synthesized CuBTC MOF and Au@CuBTC MOF.

that no vibrational bond formed between CuBTC MOF and Au nanoparticles.

Raman Spectroscopy Analysis

The Raman spectra of CuBTC MOF and Au nanoparticle incorporated CuBTC MOF are shown in **Figure 2**. The Raman spectra of CuBTC MOF shows that the Raman shift at 500 cm^{-1} corresponds to the presence of Cu(II) species, with peaks at 1,006 cm^{-1} and 1,606 cm^{-1} attributed to the ν(C=C) modes of the benzene ring. The vibrational peak at 1,457 cm^{-1} corresponds to $\nu_s(COO^-)$. This confirms the formation of CuBTC MOF (Deshmukh et al., 2018b). Au@CuBTC MOF does not show any change in the Raman spectra Au nanoparticles, does not affect the chemical bonding in CuBTC MOF, and that the Au nanoparticles are not Raman active (Worrall et al., 2016).

Structural Analysis

The structural analysis of as synthesized CuBTC and Au@CuBTC MOF carried out by X-ray diffraction is shown in **Figure 3**. All the diffraction peaks were compared and matched with the ICDD database no. PDF 00-065-1028 and reported literature (Wang et al., 2014). Both the patterns of as synthesized CuBTC and Au@CuBTC shows the same diffraction pattern and peak positions except one very small extra peak, which appeared at 2θ = 38.2°C. This confirms the presence of Au nanoparticles in the compound, while peaks in both materials represent the crystal structure of CuBTC MOF (cubic) at the 2θ angle with respective d_{hkl} planes showing 5.8° (111), 6.7° (200), 9.5° (220), 11.6° (222), 14.7° (331), 15° (420), 16.5° (422), 17.5° (333), 19,0° (440), 20.2° (442), 21.3° (620) 23.4° (444), 24.1° (551), 26.0° (553), 27.7° (733), 28.7° (660), and 35.2° (951). The crystalline size of both the compounds was calculated by classical Scherrer formula (Dastan et al., 2014) by considering peaks of the XRD patterns, as shown in **Figure 3**:

$$D = \frac{K\lambda}{\beta Cos\theta} \quad (1)$$

where D is the average crystallite size, λ is the wavelength of the X-ray radiation (λ = 1.5404 A°), K is the Scherrer constant (0.89 for cubic shape), θ is the Bragg diffraction angle, and β is the full width at half-maximum height (FWHM). The crystallinity and crystallite size of as synthesized CuBTC were found to be 74.4% and 199.94 nm, respectively, while reduction of the crystallinity and crystallite size in Au nanoparticle incorporated CuBTC MOF observed as 69.9% and 108.41 nm respectively.

Morphological Analysis

The FE-SEM images show distinct changes in morphology, particle size, and the crystalline nature of as-synthesized CuBTC, Au@CuBTC, shown in **Figures 4A,B**. **Figure 4B** indicates the presence of the Au nanoparticles in the composite on the surface, but most that the Au nanoparticles are incorporated in the MOF crystal. The elemental confirmation of the compounds was carried out using Energy-dispersive X-ray spectroscopy (EDX). Inside the CuBTC MOF structure, we recorded EDX spectra (**Figures 4C,D**) and found the presence of the Au NPs inside the CuBTC MOF, shown in **Figure 4D**. We also found the elemental concentration detail of Au@CuBTC, which is shown in **Table 1**. The CuBTC MOF has a cubic structure with a high surface area and porous morphology that provides more active sites for Au NPs inside the CuBTC MOF for the detection of Pb (II) ions sensitively.

Thermogravimetric Analysis

The thermogravimetric analysis of as-synthesized CuBTC and Au nanoparticles incorporated CuBTC is shown in **Figure 5**. In as-synthesized CuBTC, small weight loss (5.4%) started from 40 to 133°C due to the removal of H_2O molecules, while a weight loss of 29.8%, from 133 to 343°C was observed, due to the dislodgement of coordinated DMF molecules from the CuBTC MOF Structure. There was an obvious weight loss above 343°C of ∼49% in the CuBTC MOF network, which produced H_2O, CO_2, and Cu_2O, meaning that CuBTC MOF is thermally stable up to 343°C. In Au@CuBTC, a small weight loss (15.16%) started

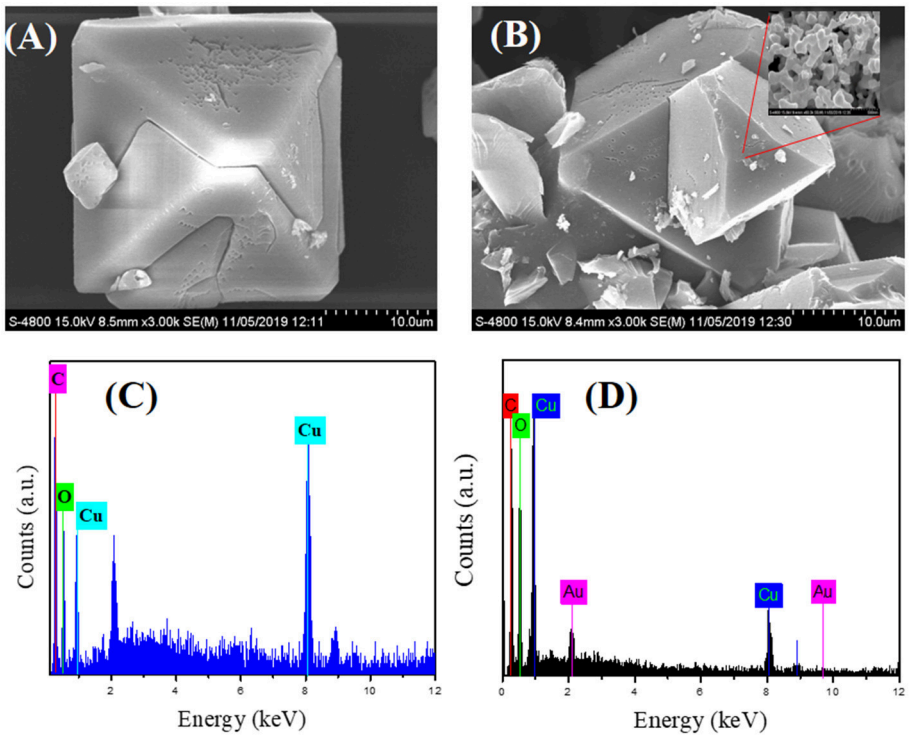

FIGURE 4 | FE-SEM images of **(A)** as-synthesized CuBTC, **(B)** Au@CuBTC, and Energy-dispersive X-ray spectroscopy (EDX) analysis of **(C)** as-synthesized CuBTC, **(D)** Au@CuBTC.

TABLE 1 | EDS elemental analysis data of as-synthesized Au@CuBTC.

Element	Atomic no.	Unnormalised concentration (wt%)	Normalized concentration (wt.%)	Atom concentration (%)	Error (wt%) (1 sigma)
Carbon (C)	6	26.05	34.19	56.28	5.50
Oxygen (O)	8	19.53	25.63	31.67	4.09
Copper (Cu)	29	28.99	38.04	11.84	1.51
Gold (Au)	79	1.63	2.14	0.22	0.16
Sum		76.21	100.00	100.00	-

from 40 to 122°C due to the removal of the H_2O molecule. A weight loss of (16.9%) from 133 to 180°C was observed, which is due to the dislodgement of coordinated DMF molecules from the Au@CuBTC MOF Structure. An obvious weight loss of ∼41.78% above 335°C was observed in Au@CuBTC MOF and produced H_2O, CO_2, and Cu_2O. These results confirm that the thermal stability of both the materials is almost the same up to ∼335°C.

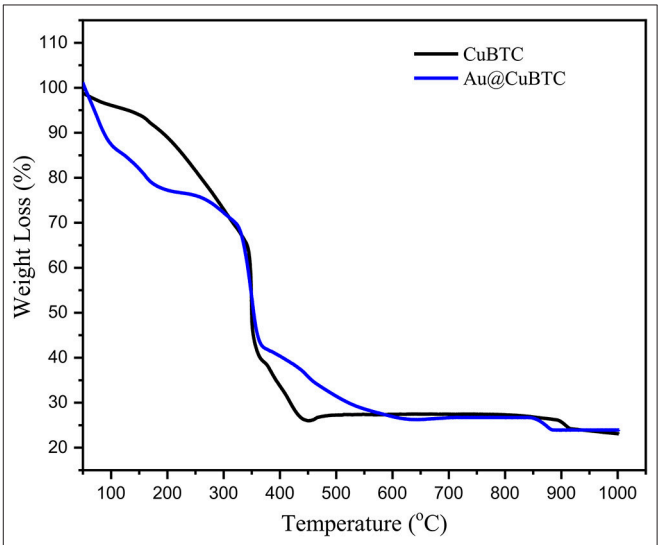

FIGURE 5 | Thermogravimetric (TGA) analysis of as synthesized CuBTC, and Au@CuBTC MOF.

Brunauer-Emmett-Teller (BET) Analysis

N_2 adsorption-desorption isotherm and BJH Pore size distribution of the as synthesized CuBTC and Au@CuBTC was studied using the Brunauer-Emmett-Teller (BET) technique, shown in **Figures 6A,B**, respectively. Both the MOFs were degassed in the Helium environment at 150°C to remove possible contaminations inside the pores. The physical adsorption of nitrogen at a temperature of 77 K was carried out for the BET surface area and pore size measurement. Both the compounds clearly show a microporous structure, having type I adsorption-desorption isotherm (Akhtar et al.,

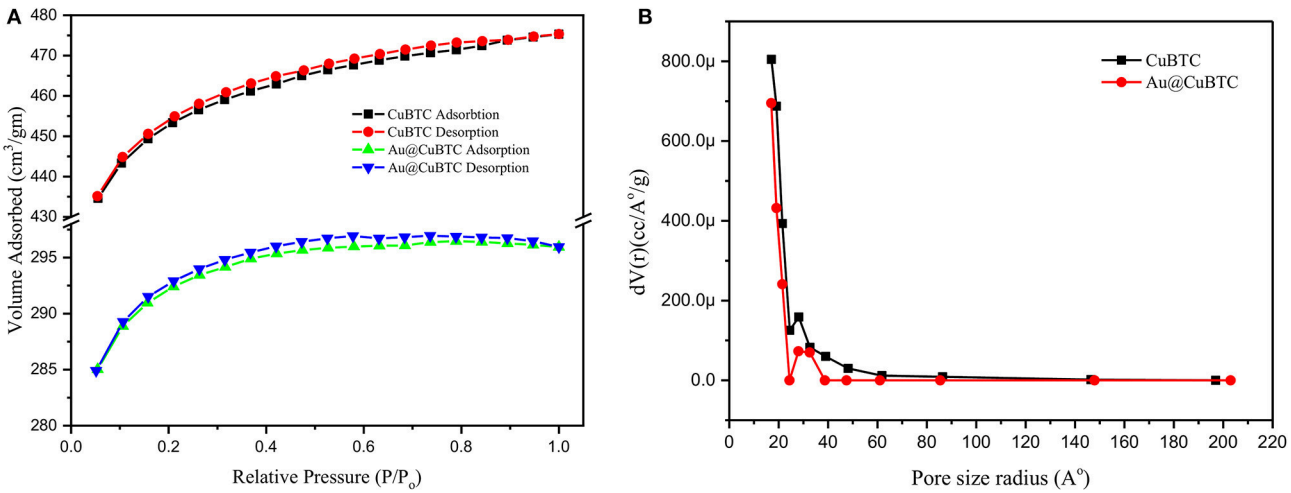

FIGURE 6 | (A) N_2 adsorption-desorption isotherm and **(B)** BJH Pore size distribution of as synthesized CuBTC and Au@CuBTC.

TABLE 2 | BET surface area details.

Compound	Surface area (m^2/gm)	Total pore volume (cc/gm)	Average pore radius (nm)
CuBTC	1374.983	0.7352	1.06942
Au@CuBTC	876.704	0.4589	1.04691

2018). The BET surface area details are shown in **Table 2**. The surface area, total pore volume, and average pore radius of Au nanoparticle incorporated CuBTC MOF reduces as compared to the synthesized CuBTC MOF.

X-ray Photoelectron Spectroscopy (XPS) Analysis

To analyze the surface chemical state of as synthesized CuBTC and Au@CuBTC, XPS measurements were performed as shown in **Figure 7**. The XPS spectra of C 1s (**Figure 7A**) shows binding energy (BE) peaks at 286.3 and 290.2 eV of as synthesized CuBTC and Au@CuBTC, with the same BE of C 1s. This indicates no interaction between Au nanoparticle and CuBTC at the carbon site. The XPS spectra at Cu 2p (**Figure 7B**) of as synthesized CuBTC and Au@CuBTC shows the same spectrum having a small decrease in peak intensity of Au@CuBTC, which may be due to the presence of Au nanoparticles inside the CuBTC. The peaks present in both the compounds at 936.2 eV and 956.3 eV correspond to Cu 2p3/2 and Cu 2p1/2, with shake-up satellite bands that confirm the +2 oxidation state (Luo et al., 2016). The spectra of O 1s (**Figure 7C** in both the compound shows no change in the chemical states of oxygen after incorporation with Au nanoparticles in CuBTC. The peak at BE of 533.4 eV indicates the presence of carboxylic species in CuBTC. **Figure 7D** shows the XPS spectra of Au@CuBTC at the binding energy edge of Au 4f and confirms the presence of Au nanoparticles in CuBTC, with the peaks at 87.30 and 94.70 eV attributed to the Au 4f5/2 and Au 4f7/2 transitions (Ghodake et al., 2010).

Electrochemical Analysis

The electrochemical activity of bare GCE, Au Np, CuBTC, and Au@CuBTC were studied by cyclic voltammetry in a 10 mM $[Fe(CN)_6]^{3-/4-}$ solution containing 0.1 M KCl solution at a scan rate of 100 mV/s, as shown in **Figure 8**. The CuBTC coated glassy carbon electrode (GCE) shows distinct oxidation and reduction peaks at 0.02 and −0.5 V versus Ag/AgCl reference electrode, indicating the reversible oxidation and reduction of Cu(II) to Cu(I) (Kumar et al., 2012). The CV curve of the Au@CuBTC coated GCE electrode shows a distinct reduction peak compared with pure CuBTC and the same oxidation peak, with an increase in oxidation current that probably an overlapping of the oxidation of Au nanoparticles over CuBTC MOF, while bare GCE and Au Np coated GCE shows higher current due to high conductivity.

Bare GCE, Au Np, CuBTC, and Au@CuBTC were characterized by EIS, which is an effective tool to study electrochemical activity by applying variable AC frequencies. The EIS spectra of bare GCE, Au Np, CuBTC, and Au@CuBTC coated films on GCE were recorded in the AC frequency range of 0.01 Hz to 0.1 MHz in a 10 mM $[Fe(CN)_6]^{3-/4-}$ solution containing 0.1 M KCl. Nyquist plot (**Figure 9**) showed a slight decrease in a semicircle of Au@CuBTC as compared to CuBTC, which is due to a slight increase in the ionic conductivity in CuBTC after the incorporation of Au nanoparticles due to the small concentration of Au NPs, and a slight difference was observed. Bare GCE and Au Np showed a very small semicircle due to the very low electron transfer resistance (Ret) of the redox probe. The increase in diameter of the semicircle in the CuBTC MOF and Au@CuBTC MOF modified GCE surface was due to the insulating nature of CuBTC MOF which acts as a barrier for the electrochemical process and slowed down the diffusion of the electrochemical probe toward the electrode surface. EIS and CV results are complementary to each other.

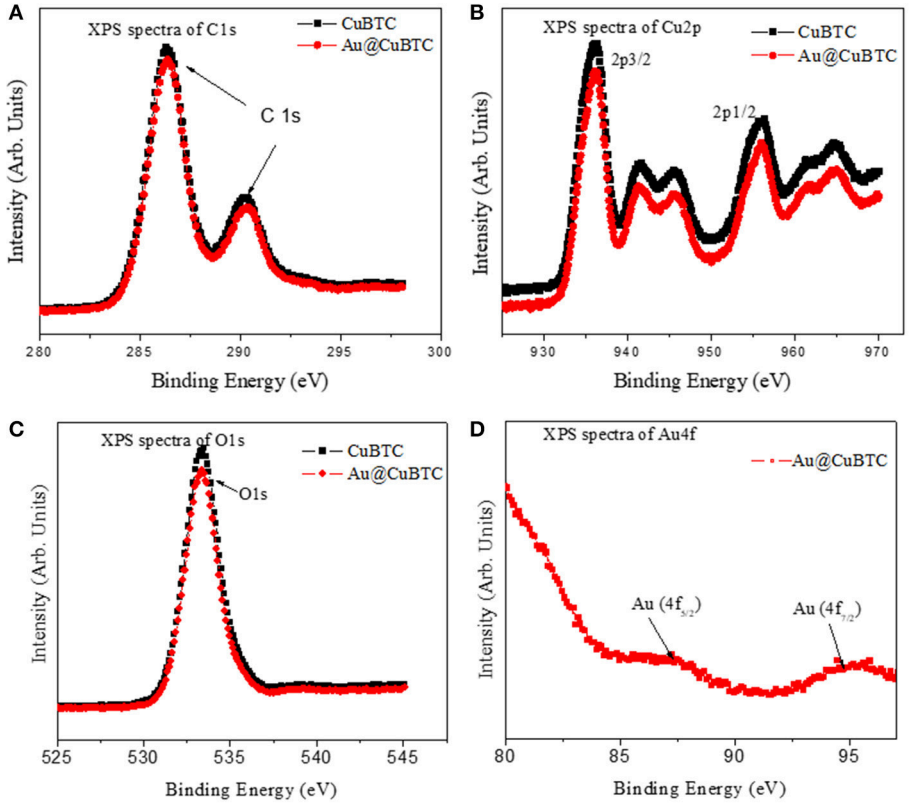

FIGURE 7 | XPS spectra of **(A)** C1s **(B)** Cu2p **(C)** O1s of CuBTC and Au@CuBTC and **(D)** Au4f of Au@CuBTC.

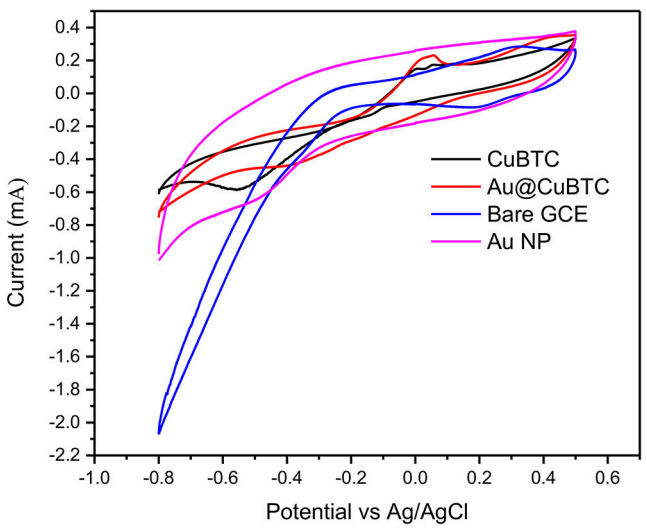

FIGURE 8 | Cyclic voltammograms (CV) of bare GCE, Au NP, CuBTC MOF, and Au@CuBTC MOF.

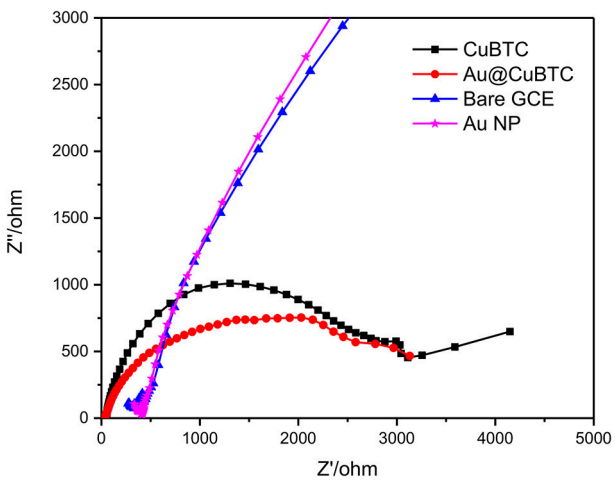

FIGURE 9 | Electrochemical Impedance Spectroscopy (EIS) Nyquist plot of bare GCE, Au NP, CuBTC MOF, and Au@CuBTC MOF.

SENSOR PERFORMANCE

The sensing experiment was carried out in two steps: (1) Accumulation in Pb^{2+} ions solution, and (2) reduction in buffer solution by applying differential pulse voltammetry (DPV), where the accumulated Pb^{2+} ions can get reduced at particular potential Pb^{2+} ions (Equation 1). As shown in **Figure 10A**, the bare GCE Au nanoparticles coated GCE and CuBTC shows lower response to the Pb^{2+} ions at a concentration of

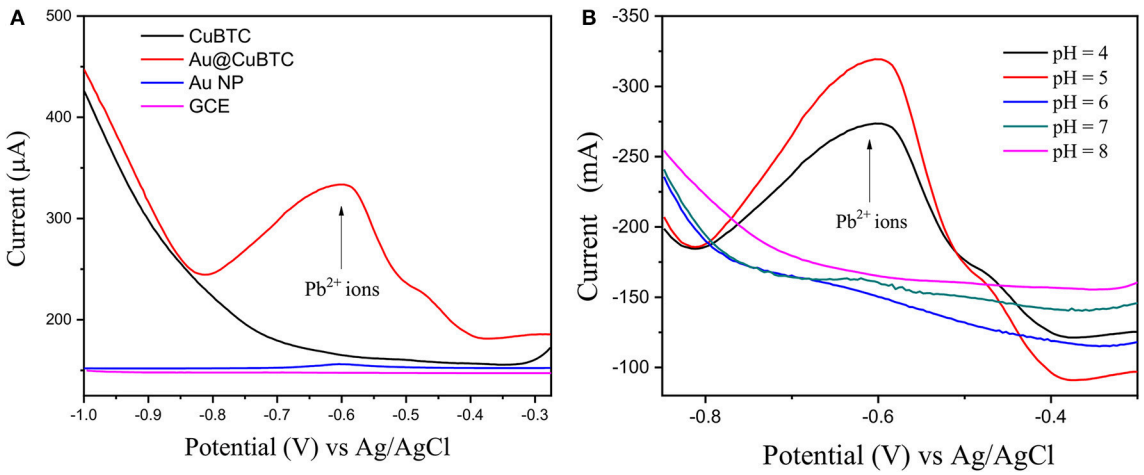

FIGURE 10 | (A) Differential pulse voltammograms (DPV) of 0.01 mMol L^{-1} Pb (II) ions in acetate buffer (pH-5) of bare GCE, Au Nps, CuBTC, and Au@CuBTC and **(B)** DPV of Au@CuBTC to 1 μM/L Pb^{2+} ions at various pH.

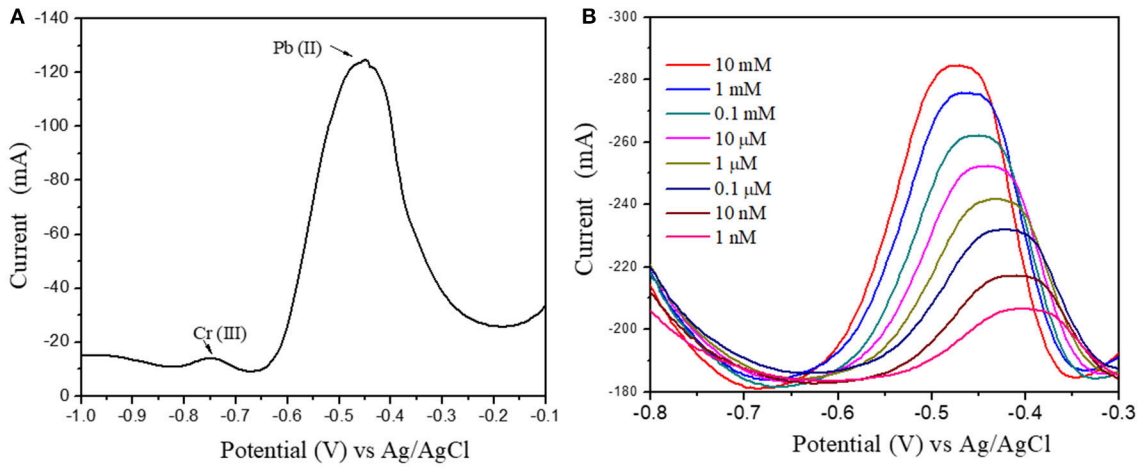

FIGURE 11 | (A) Pb(II) and Cr(III) ions DPV response at 1 μM concentration **(B)** Differential Pulse Voltammograms of Au@CuBTC modified GCE electrodes for Pb(II) ions concentration of 10 mM/L to 1 nM/L.

0.01 mM/L. However, Au@CuBTC shows a significant sensing response to the Pb^{2+} ions, which means that after incorporating Au nanoparticles in CuBTC become sensitive toward Pb^{2+} ions. The Au Np work as a catalyst while the CuBTC MOF provides more surface area and the pore provides more active sites for electrocatalytic activity, which enables highly sensitive detection of Pb^{2+} ions. Here, in the accumulation step, Pb^{2+} ions coordinate with Au@CuBTC MOF and form PbO that are trapped on the surface of Au@CuBTC MOF, while in the DPV they are reduced at the reduction potential (Equation 1) (Metzger, 2012), which results in a large flow of current through working and counter electrodes as shown in **Figures 10**, **11**.

$$PbO_{(s)} + H_2O(l) + 2e^{-1} \rightarrow Pb_{(s)} + 2OH^{-1}_{(aq)}$$
$$E^{\circ} = -0.58V \quad (1)$$

Figure 10B shows the DPV curve of Pb^{2+} ions at the concentration of 1 μM/L at the various pH (4–8) and shows the highest sensitivity at pH 5. All the sensing experiments were carried out in acetate buffer at pH 5. The Au@CuBTC modified GCE electrode was tested for Cr^{3+} ions and Pb^{2+} ions and shows a more selective response toward Pb^{2+} ions as shown in **Figure 11A**. It was also tested for various concentrations of Pb^{2+} ions in water, as shown in **Figure 11**. The Au@CuBTC shows a sensing response toward Pb^{2+} ions up to a lower detection limit of 1 nM/L, which is below the Maximum Contamination Level (MCL) of 0.03 μM/L as proposed by EPA, USA (Landmeyer et al., 2003). The comparative studies for the detection of Pb(II) ions by electrochemical method using various materials are shown in **Table 3**. This indicates that this work has a better deletion limit (LOD) compared to other reported

TABLE 3 | Comparative studies for detection of Pb(II) ions by electrochemical method using various materials.

Sr. No.	Sensing material electrode	Sensing technique	Detection limit (LOD) of Pb^{2+} ions	References
1.	Bismuth/Poly(1,8-diaminonaphthalene) modified carbon paste electrode (CPE)	Square-wave voltammetry	0.3 μg L^{-1}	Salih et al., 2017
2.	Bismuth-Carbon pate electrode (CPE)	Square-wave anodic stripping voltammetry	0.3 μg/L	Martín-Yerga et al., 2017
3.	Glassy carbon electrode modified SWNTs/Biomass electrode	Differential pulse anodic stripping voltammetry	10^{-8} M	Dali et al., 2018
4.	TAPB-DMTP-COF (TAPB, 1,3,5-tris(4-aminophenyl)benzene; DMTP, 2,5-dimethoxyterephaldehyde; COF, covalent organic framework) modified carbon paste electrode	Differential pulse anodic stripping voltammetry	1.9 nmol/L	Zhang et al., 2018
5.	Iron oxide (Fe_3O_4) nanoparticles (NPs) capped with terephthalic acid (TA)/Glassy Carbon Electrode	Square wave anodic stripping voltammetry	0.05 μM/L	Deshmukh et al., 2017
6.	EDTA-Ppy/SWNTs modified stainless steel electrode	Differential pulse voltammetry	0.15 μM/L	Deshmukh et al., 2018a
7.	Fe_3O_4@PDA@MnO_2 electrode	Differential pulse voltammetry	0.03 μg L^{-1}	Wang et al., 2020
8.	Au@CuBTC MOF modified GCE electrodes	Differential pulse voltammetry	1 nM/L	This work

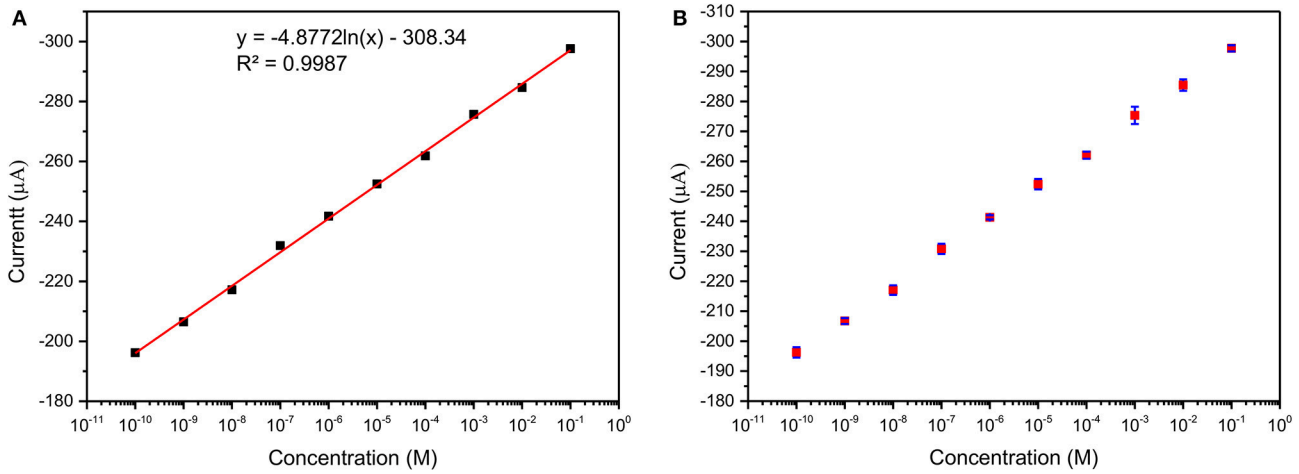

FIGURE 12 | (A) Calibration plot and **(B)** Error bar diagram of Au@CuBTC modified GCE electrodes for Pb(II) ions concentration of 10 mM/L to 1 nM/L.

data. The calibration plot and error bar diagram also show (**Figures 12A,B**) that the fabricated sensor shows good linearity and repeatability.

CONCLUSIONS

In this study successfully synthesized and rigorously characterized CuBTC MOF and Au nanoparticle incorporated CuBTC MOF (Au@CuBTC). We prepared an electrochemical sensor based on Au@CuBTC MOF that showed a significant response and sensitivity toward Pb^{2+} ions compared with pure CuBTC MOF coated on the GCE electrode. Au@CuBTC MOF shows the highest sensitivity in acetate buffer at pH 5 and shows great affinity toward Pb^{2+} ions in water media at a lower detection limit of 1 nM/L concentration at pH 5.0 by using a DPV technique which is far below the Maximum Contamination Level (MCL) as proposed by EPA, USA.

DATA AVAILABILITY STATEMENT

The raw data supporting the conclusions of this article will be made available by the authors, without undue reservation.

AUTHOR CONTRIBUTIONS

GB and BH contributed equally in experimental work, idea generation, and data analysis. MD and HP contributed for electrochemical experiment data analysis. SMS contributed in experimental work. DP and KP contributed for XPS and XRD experimental data collection analysis. MS contributed as

corresponding author (i.e., idea, experiment, data validation, and guidance). All authors contributed to the article and approved the submitted version.

ACKNOWLEDGMENTS

The authors extend their sincere thanks to the following for providing financial support: UGC—DAE CSR (RRCAT), Indore (Project No. CSR-IC-BL66/CRS- 183/2016-17/847), Inter University Accelerator Center (IUAC), New Delhi, India (UFR no. 62320), DST—SERB, New Delhi (Project No. EEQ/2017/000645), Rashtria Uchachatar Shiksha Abhiyan (RUSA), Government of Maharashtra, UGC-SAP Programme (F.530/16/DRS-I/2016 (SAP-II) Dt.16-04-2016), and DST-FIST (Project No. SR/FST/PSI-210/2016(C) dtd. 16/12/2016).

REFERENCES

Akhtar, S., Bala, S., De, A., Das, K. S., Adhikary, A., Jyotsna, S., et al. (2018). Designing multifunctional MOFs using the inorganic motif [Cu3 (μ3-OH)(μ-Pyz)] as an SBU and their properties. *Crystal Growth Design* 19, 992–1004. doi: 10.1021/acs.cgd.8b01540

Ali, I., and Aboul-Enein, H. Y. (2002). Speciation of arsenic and chromium metal ions by reversed phase high performance liquid chromatography. *Chemosphere* 48, 275–278. doi: 10.1016/S0045-6535(02)00085-1

Bodkhe, G. A., Deshmukh, M. A., Patil, H. K., Shirsat, S. M., Srihari, V., Pandey, K. K., et al. (2019). Field effect transistor based on proton conductive metal organic framework (CuBTC). *J. Phys.* 52:335105. doi: 10.1088/1361-6463/ab1987

Butova, V. V., Kirichkov, M. V., Budnyk, A. P., Guda, A. A., Soldatov, M. A., Lamberti, C., et al. (2018). A room-temperature growth of gold nanoparticles on MOF-199 and its transformation into the $[Cu_2(OH)(BTC)(H_2O)]$ n phase. *Polyhedron* 154, 357–363. doi: 10.1016/j.poly.2018.08.002

Chen, S., Li, Y., and Mi, L. (2020). Porous carbon derived from metal organic framework for gas storage and separation: the size effect. *Inorg. Chem. Commun.* 118:107999. doi: 10.1016/j.inoche.2020.107999

Cobben, P. L., Egberink, R. J., Bomer, J. G., Bergveld, P., Verboom, W., and Reinhoudt, D. N. (1992). Transduction of selective recognition of heavy metal ions by chemically modified field effect transistors (CHEMFETs). *J. Am. Chem. Soc.* 114, 10573–10582. doi: 10.1021/ja00052a063

Cui, L., Wu, J., and Ju, H. (2015). Electrochemical sensing of heavy metal ions with inorganic, organic and bio-materials. *Biosens. Bioelectr.* 63, 276–286. doi: 10.1016/j.bios.2014.07.052

Dai, H., Wang, N., Wang, D., Ma, H., and Lin, M. (2016). An electrochemical sensor based on phytic acid functionalized polypyrrole/graphene oxide nanocomposites for simultaneous determination of Cd (II) and Pb (II). *Chem. Eng. J.* 299, 150–155. doi: 10.1016/j.cej.2016.04.083

Dali, M., Zinoubi, K., Chrouda, A., Abderrahmane, S., Cherrad, S., and Jaffrezic-Renault, N. (2018). A biosensor based on fungal soil biomass for electrochemical detection of lead (II) and cadmium (II) by differential pulse anodic stripping voltammetry. *J. Electroanal. Chem.* 813, 9–19. doi: 10.1016/j.jelechem.2018.02.009

Dastan, D., Londhe, P. U., and Chaure, N. B. (2014). Characterization of TiO_2 nanoparticles prepared using different surfactants by sol–gel method. *J. Mater. Sci.* 25, 3473–3479. doi: 10.1007/s10854-014-2041-9

Dastan, D., Panahi, S. L., and Chaure, N. B. (2016). Characterization of titania thin films grown by dip-coating technique. *J. Mater. Sci.* 27, 12291–12296. doi: 10.1007/s10854-016-4985-4

Deshmukh, M. A., Bodkhe, G. A., Shirsat, S., Ramanavicius, A., and Shirsat, M. D. (2018a). Nanocomposite platform based on EDTA modified Ppy/SWNTs for the sensing of Pb (II) ions by electrochemical method. *Front. Chem.* 6:451. doi: 10.3389/fchem.2018.00451

Deshmukh, M. A., Celiesiute, R., Ramanaviciene, A., Shirsat, M. D., and Ramanavicius, A. (2018b). EDTA_PANI/SWCNTs nanocomposite modified electrode for electrochemical determination of copper (II), lead (II) and mercury (II) ions. *Electrochim. Acta* 259, 930–938. doi: 10.1016/j.electacta.2017.10.131

Deshmukh, M. A., Patil, H. K., Bodkhe, G. A., Yasuzawa, M., Koinkar, P., Ramanaviciene, A., et al. (2018c). EDTA-modified PANI/SWNTs nanocomposite for differential pulse voltammetry based determination of Cu (II) ions. *Sensors Actuat. B* 260, 331–338. doi: 10.1016/j.snb.2017.12.160

Deshmukh, M. A., Patil, H. K., Bodkhe, G. A., Yasuzawa, M., Koinkar, P., Ramanavicius, A., et al. (2018d). EDA modified PANI/SWNTs nanocomposite for determination of Ni (II) metal ions. *Colloid. Surf. A* 537, 303–309. doi: 10.1016/j.colsurfa.2017.10.026

Deshmukh, M. A., Shirsat, M. D., Ramanaviciene, A., and Ramanavicius, A. (2018e). Composites based on conducting polymers and carbon nanomaterials for heavy metal ion sensing. *Crit. Rev. Anal. Chem.* 48, 293–304. doi: 10.1080/10408347.2017.1422966

Deshmukh, S., Kandasamy, G., Upadhyay, R. K., Bhattacharya, G., Banerjee, D., Maity, D., et al. (2017). Terephthalic acid capped iron oxide nanoparticles for sensitive electrochemical detection of heavy metal ions in water. *J. Electroanal. Chem.* 788, 91–98. doi: 10.1016/j.jelechem.2017.01.064

Faraji, M., Yamini, Y., Saleh, A., Rezaee, M., Ghambarian, M., and Hassani, R. (2010). A nanoparticle-based solid-phase extraction procedure followed by flow injection inductively coupled plasma-optical emission spectrometry to determine some heavy metal ions in water samples. *Anal. Chim. Acta* 659, 172–177. doi: 10.1016/j.aca.2009.11.053

Forzani, E. S., Zhang, H., Chen, W., and Tao, N. (2005). Detection of heavy metal ions in drinking water using a high-resolution differential surface plasmon resonance sensor. *Environ. Sci. Technol.* 39, 1257–1262. doi: 10.1021/es049234z

Fu, F., and Wang, Q. (2011). Removal of heavy metal ions from wastewaters: a review. *J. Environ. Manag.* 92, 407–418. doi: 10.1016/j.jenvman.2010.11.011

Ghodake, G., Deshpande, N., Lee, Y., and Jin, E. (2010). Pear fruit extract-assisted room-temperature biosynthesis of gold nanoplates. *Colloid. Surf. B* 75, 584–589. doi: 10.1016/j.colsurfb.2009.09.040

Golsheikh, A. M., Yeap, G.-Y., Yam, F. K., and San Lim, H. (2020). Facile fabrication and enhanced properties of copper-based metal organic framework incorporated with graphene for non-enzymatic detection of hydrogen peroxide. *Synthetic Metals* 260:116272. doi: 10.1016/j.synthmet.2019.116272

Han, Y., Han, L., Zhang, L., and Dong, S. (2015). Ultrasonic synthesis of highly dispersed Au nanoparticles supported on Ti-based metal–organic frameworks for electrocatalytic oxidation of hydrazine. *J. Mater. Chem. A* 3, 14669–14674. doi: 10.1039/C5TA03090K

Hung, Y.-L., Hsiung, T.-M., Chen, Y.-Y., Huang, Y.-F., and Huang, C.-C. (2010). Colorimetric detection of heavy metal ions using label-free gold nanoparticles and alkanethiols. *J. Phys. Chem. C* 114, 16329–16334. doi: 10.1021/jp1061573

Hwang, G.-H., Han, W.-K., Park, J.-S., and Kang, S.-G. (2008). An electrochemical sensor based on the reduction of screen-printed bismuth oxide for the determination of trace lead and cadmium. *Sensors Actuat. B* 135, 309–316. doi: 10.1016/j.snb.2008.08.039

Ishida, T., Nagaoka, M., Akita, T., and Haruta, M. (2008). Deposition of gold clusters on porous coordination polymers by solid grinding and their catalytic activity in aerobic oxidation of alcohols. *Chem. Eur. J.* 14, 8456–8460. doi: 10.1002/chem.200800980

Jiang, H.-L., Liu, B., Akita, T., Haruta, M., Sakurai, H., and Xu, Q. (2009). Au@ZIF-8: CO oxidation over gold nanoparticles deposited to metal—organic framework. *J. Am. Chem. Soc.* 131, 11302–11303. doi: 10.1021/ja9047653

Ke, F., Wang, L., and Zhu, J. (2015). Multifunctional Au-Fe 3 O 4@ MOF core–shell nanocomposite catalysts with controllable reactivity and magnetic recyclability. *Nanoscale* 7, 1201–1208. doi: 10.1039/C4NR05421K

Kim, Y., Johnson, R. C., and Hupp, J. T. (2001). Gold nanoparticle-based sensing of "spectroscopically silent" heavy metal ions. *Nano Lett.* 1, 165–167. doi: 10.1021/nl0100116

Kimmel, D. W., LeBlanc, G., Meschievitz, M. E., and Cliffel, D. E. (2011). Electrochemical sensors and biosensors. *Anal. Chem.* 84, 685–707. doi: 10.1021/ac202878q

Kumar, R. S., Kumar, S. S., and Kulandainathan, M. A. (2012). Highly selective electrochemical reduction of carbon dioxide using Cu based metal organic framework as an electrocatalyst. *Electrochem. Commun.* 25, 70–73. doi: 10.1016/j.elecom.2012.09.018

Landmeyer, J., Bradley, P., and Bullen, T. (2003). Stable lead isotopes reveal a natural source of high lead concentrations to gasoline-contaminated groundwater. *Environ. Geol.* 45, 12–22. doi: 10.1007/s00254-003-0863-5

Lee, J., Farha, O. K., Roberts, J., Scheidt, K. A., Nguyen, S. T., and Hupp, J. T. (2009). Metal–organic framework materials as catalysts. *Chem. Soc. Rev.* 38, 1450–1459. doi: 10.1039/b807080f

Lin, R.-B., Xiang, S., Zhou, W., and Chen, B. (2020). Microporous metal-organic framework materials for gas separation. *Chem* 6, 337–363. doi: 10.1016/j.chempr.2019.10.012

Lin, S., Song, Z., Che, G., Ren, A., Li, P., Liu, C., et al. (2014). Adsorption behavior of metal–organic frameworks for methylene blue from aqueous solution. *Micropor. Mesopor. Mater.* 193, 27–34. doi: 10.1016/j.micromeso.2014.03.004

Liu, L., Zhou, Y., Liu, S., and Xu, M. (2018). The applications of metal–organic frameworks in electrochemical sensors. *ChemElectroChem* 5, 6–19. doi: 10.1002/celc.201700931

Luo, Q.-x., Ji, M., Park, S.-E., Hao, C., and Li, Y.-q. (2016). PdCl 2 immobilized on metal–organic framework CuBTC with the aid of ionic liquids: enhanced catalytic performance in selective oxidation of cyclohexene. *RSC Adv.* 6, 33048–33054. doi: 10.1039/C6RA02077A

Maleki, A. (2018). Green oxidation protocol: Selective conversions of alcohols and alkenes to aldehydes, ketones and epoxides by using a new multiwall carbon nanotube-based hybrid nanocatalyst *via* ultrasound irradiation. *Ultrasonics Sonochem.* 40, 460–464. doi: 10.1016/j.ultsonch.2017.07.020

Maleki, A., Hajizadeh, Z., and Firouzi-Haji, R. (2018). Eco-friendly functionalization of magnetic halloysite nanotube with SO3H for synthesis of dihydropyrimidinones. *Micropor. Mesopor. Mater.* 259, 46–53. doi: 10.1016/j.micromeso.2017.09.034

Maleki, A., Hajizadeh, Z., Sharifi, V., and Emdadi, Z. (2019). A green, porous and eco-friendly magnetic geopolymer adsorbent for heavy metals removal from aqueous solutions. *J. Clean. Prod.* 215, 1233–1245. doi: 10.1016/j.jclepro.2019.01.084

Maleki, A., Rahimi, R., and Maleki, S. (2016). Efficient oxidation and epoxidation using a chromium (VI)-based magnetic nanocomposite. *Environ. Chem. Lett.* 14, 195–199. doi: 10.1007/s10311-016-0558-2

Martín-Yerga, D., Alvarez-Martos, I., Blanco-Lopez, M. C., Henry, C. S., and Fernández-Abedul, M. T. (2017). Point-of-need simultaneous electrochemical detection of lead and cadmium using low-cost stencil-printed transparency electrodes. *Anal. Chim. Acta* 981, 24–33. doi: 10.1016/j.aca.2017.05.027

Marx, S., Kleist, W., and Baiker, A. (2011). Synthesis, structural properties, and catalytic behavior of Cu-BTC and mixed-linker Cu-BTC-PyDC in the oxidation of benzene derivatives. *J. Catalysis* 281, 76–87. doi: 10.1016/j.jcat.2011.04.004

Meena, A. K., Mishra, G., Rai, P., Rajagopal, C., and Nagar, P. (2005). Removal of heavy metal ions from aqueous solutions using carbon aerogel as an adsorbent. *J. Hazard. Mater.* 122, 161–170. doi: 10.1016/j.jhazmat.2005.03.024

Meng, Z., Li, M., Liu, X., and Lei, Z. (2019). Sensitive electrochemical sensor for hydrazine based on in situ synthesis of Cu 3 (BTC) 2/GO nanocomposite. *J. Mater. Sci.* 30, 18617–18625. doi: 10.1007/s10854-019-02214-y

Metzger, R. M. (2012). *The Physical Chemist's Toolbox.* Hoboken, NJ: John Wiley & Sons. doi: 10.1002/9781118195598

Neupane, L. N., Thirupathi, P., Jang, S., Jang, M. J., Kim, J. H., and Lee, K.-H. (2011). Highly selectively monitoring heavy and transition metal ions by a fluorescent sensor based on dipeptide. *Talanta* 85, 1566–1574. doi: 10.1016/j.talanta.2011.06.052

Quang, D. T., and Kim, J. S. (2010). Fluoro-and chromogenic chemodosimeters for heavy metal ion detection in solution and biospecimens. *Chem. Rev.* 110, 6280–6301. doi: 10.1021/cr100154p

Rauf, S., Vijjapu, M. T., Andres, M. A., Gascón, I., Roubeau, O., Eddaoudi, M., et al. (2020). A highly selective metal-organic framework textile humidity sensor. *ACS Appl. Mater. Interfaces.* 12:29999–30006. doi: 10.1021/acsami.0c07532

Roushani, M., Valipour, A., and Saedi, Z. (2016). Electroanalytical sensing of Cd2+ based on metal–organic framework modified carbon paste electrode. *Sensors Actuat. B* 233, 419–425. doi: 10.1016/j.snb.2016.04.106

Salih, F. E., Ouarzane, A., and El Rhazi, M. (2017). Electrochemical detection of lead (II) at bismuth/poly (1, 8-diaminonaphthalene) modified carbon paste electrode. *Arab. J. Chem.* 10, 596–603. doi: 10.1016/j.arabjc.2015.08.021

Saraf, M., Rajak, R., and Mobin, S. M. (2016). A fascinating multitasking Cu-MOF/rGO hybrid for high performance supercapacitors and highly sensitive and selective electrochemical nitrite sensors. *J. Mater. Chem. A* 4, 16432–16445. doi: 10.1039/C6TA06470A

Singh, R., Gautam, N., Mishra, A., and Gupta, R. (2011). Heavy metals and living systems: an overview. *Indian J. Pharmacol.* 43:246. doi: 10.4103/0253-7613.81505

Tan, E., Yin, P., Lang, X., Zhang, H., and Guo, L. (2012). A novel surface-enhanced Raman scattering nanosensor for detecting multiple heavy metal ions based on 2-mercaptoisonicotinic acid functionalized gold nanoparticles. *Spectrochim. Acta A* 97, 1007–1012. doi: 10.1016/j.saa.2012.07.114

Travlou, N. A., Singh, K., Rodríguez-Castellón, E., and Bandosz, T. J. (2015). Cu–BTC MOF–graphene-based hybrid materials as low concentration ammonia sensors. *J. Mater. Chem. A* 3, 11417–11429. doi: 10.1039/C5TA01738F

Wang, L., Lei, T., Ren, Z., Jiang, X., Yang, X., Bai, H., et al. (2020). Fe3O4@ PDA@ MnO2 core-shell nanocomposites for sensitive electrochemical detection of trace Pb (II) in water. *J. Electroanal. Chem.* 864:114065. doi: 10.1016/j.jelechem.2020.114065

Wang, Y., Ge, H., Wu, Y., Ye, G., Chen, H., and Hu, X. (2014). Construction of an electrochemical sensor based on amino-functionalized metal-organic frameworks for differential pulse anodic stripping voltammetric determination of lead. *Talanta* 129, 100–105. doi: 10.1016/j.talanta.2014.05.014

Worrall, S. D., Bissett, M. A., Hill, P. I., Rooney, A. P., Haigh, S. J., Attfield, M. P., et al. (2016). Metal-organic framework templated electrodeposition of functional gold nanostructures. *Electrochim. Acta* 222, 361–369. doi: 10.1016/j.electacta.2016.10.187

Wu, G., Kang, H., Zhang, X., Shao, H., Chu, L., and Ruan, C. (2010). A critical review on the bio-removal of hazardous heavy metals from contaminated soils: issues, progress, eco-environmental concerns and opportunities. *J. Hazard. Mater.* 174, 1–8. doi: 10.1016/j.jhazmat.2009.09.113

Wuttke, S., Zimpel, A., Bein, T., Braig, S., Stoiber, K., Vollmar, A., et al. (2017). Validating metal-organic framework nanoparticles for their nanosafety in diverse biomedical applications. *Adv. Healthcare Mater.* 6:1600818. doi: 10.1002/adhm.201600818

Yadav, D. K., Gupta, R., Ganesan, V., Sonkar, P. K., and Yadav, M. (2018). Gold nanoparticles incorporated in a zinc-based metal-organic framework as multifunctional catalyst for the oxygen reduction and hydrogen evolution reactions. *ChemElectroChem* 5, 2612–2619. doi: 10.1002/celc.201800519

Zhang, C., Wang, M., Liu, L., Yang, X., and Xu, X. (2013). Electrochemical investigation of a new Cu-MOF and its electrocatalytic activity towards H_2O_2 oxidation in alkaline solution. *Electrochem. Commun.* 33, 131–134. doi: 10.1016/j.elecom.2013.04.026

Zhang, T., Gao, C., Huang, W., Chen, Y., Wang, Y., and Wang, J. (2018). Covalent organic framework as a novel electrochemical platform for highly sensitive and stable detection of lead. *Talanta* 188, 578–583. doi: 10.1016/j.talanta.2018.06.032

Zhou, J., Li, X., Yang, L., Yan, S., Wang, M., Cheng, D., et al. (2015). The Cu-MOF-199/single-walled carbon nanotubes modified electrode for simultaneous determination of hydroquinone and catechol with extended linear ranges and lower detection limits. *Anal. Chim. Acta* 899, 57–65. doi: 10.1016/j.aca.2015.09.054

Conflict of Interest: The authors declare that the research was conducted in the absence of any commercial or financial relationships that could be construed as a potential conflict of interest.